Photonic integrated circuits for terahertz source generation

Lianping Hou*, Song Tang, Bin Hou, John H. Marsh

James Watt School of Engineering, University of Glasgow, Glasgow, G12 8QQ, U.K
*Lianping.hou@glasgow.ac.uk

Abstract: We introduce four kinds of terahertz photonics components based on photonic integrated circuits (PICs). A PIC-based integrated optoelectronic synthesizer for THz communications is described, which can be tuned continuously over the range 0.254 THz to 2.723 THz using photomixing. A laterally-coupled dual-grating distributed feedback laser (DFB) diode integrated with an electroabsorption modulator is used to generate an 820 GHz beat signal. THz signal production is reported using a dual-wavelength DFB diode laser with a two-section phase-shifted sampled Bragg grating. Finally, a THz source at 640 GHz, based on a sampled grating distributed Bragg reflector semiconductor mode-locked laser diode, is reported offering superior reproducibility, controllability and a wider operation range than other reported mode-locked THz laser diodes. Each of these sources is a monolithic construction emitting light at 1.5 µm. The light can be amplified in an EDFA, delivered over silica optical fibre and used to generate THz radiation via a photodiode antenna or photoconductive antenna in a remote location.

1. Introduction

THz radiation (0.1-10 THz) has many applications, including medical imaging [1], spectroscopy [2], security screening [3], detection of hidden explosives, remote sensing of chemicals and of the atmosphere and high-bandwidth wireless communications. Many applications of THz radiation require sources that are compact, low-cost, and operate at room temperature. Using semiconductor technologies to produce terahertz sources has the advantages of small form factor and high energy efficiency compared to their solid-state laser counterparts, paving the way towards compact room temperature terahertz sources. This will extend the applications of THz radiation, to areas such as data storage, and ultra-high speed on-chip, data centre, and satellite to satellite communications.

One of the methods used to produce continuous THz waves is photomixing beams from two distributed feedback (DFB) semiconductor diode lasers with different wavelengths [4]. The relative wavelength drift and uncorrelated phase noise of the two sources result in terahertz signals with poor long-term stability and large phase noise. Monolithic and hybrid integration of dual-wavelength diode laser (DWL) sources increase compactness and the correlation between the lasing modes, so signals can be generated with reduced phase noise [5]. Amid the various reported configurations of DWLs, simultaneous emission of two longitudinal modes within the same cavity is particularly attractive because the beam path and polarization of the two modes are automatically matched, and the beating frequency is largely insensitive to temperature variations of the surroundings [5, 6, 7]. A second approach for generating THz pulses is to use ultrafast semiconductor mode locked laser diodes (SMLLDs) operating at THz repetition frequencies. In both the DWL and SMLLD techniques reported here, the output light from the laser is used to pump a photoconductive antenna (PCA), generating THz radiation through photomixing.

Photonic integrated circuits (PICs) are the next logical step in the world of optics and can be used in THz applications. Here we will introduce four kinds of PIC-based photonic sources that can be used to generate terahertz signals though photomixing: 1) an optoelectronic synthesizer for THz communications which can be tuned continuously from 0.254 to 2.723 THz [8]; 2) a dual-grating DWL DFB laser stabilised by four wave mixing (FWM) in an integrated electroabsorption modulator (EAM) where the lasing lines are separated by THz frequencies [6, 9]; 3) a DWL using a sampled Bragg grating with a π-phase-shifted seed grating filling half of the sampling period [10]; 4) a THz source based on sampled grating distributed Bragg reflectors (SGDBR) SMLLDs [11, 12]. In all of these PIC devices, the THz wave can be generated through difference-frequency generation (DFG) in a square law detector such as photodiode or photoconductive detector [8] or optical rectification in a nonlinear crystal. Except where noted, all the devices reported here were measured at 20 °C using a thermoelectric cooler (TEC) and operated under continuous wave (CW) biasing conditions.

2. PIC devices for generating THz signals

2.1. Fully-integrated optoelectronic synthesiser

An optical micrograph of the four channel fully-integrated optoelectronic synthesiser together with coresponding scanning electron microscope (SEM) images are shown in Fig. 1 [8]. The fabrication processes and epitaxial structure are described in [13] and [14] respectively.

The optical spectrum, measured from the semiconductor optical amplifier (SOA) side of the PIC, with all four DFB lasers working concurrently, is shown in Fig

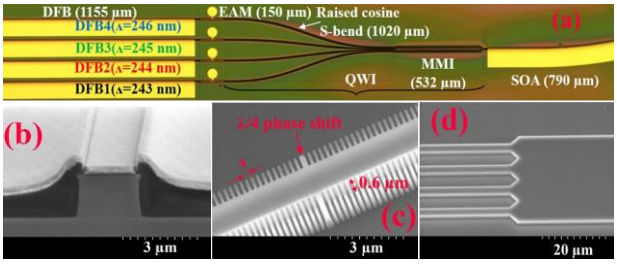

Fig. 1. Optical micrograph and SEM images of the THz frequency synthesiser.

2(a). To ensure single longitudinal mode operation of each DFB laser, a λ/4 phase shift was introduced in the middle of the DFB laser cavity. DFB1 was chosen as the base laser; three different communication channels based on the THz mixing frequencies could consequently be selected. The output power of each DFB laser could be controlled and modulated individually by using its EAM and, in order to obtain a high-quality beating signal, the power difference between the laser beam from any two DFB lasers should be no more than 2 dB, which was also the operating condition for the autocorrelation measurements reported here.

As shown in Fig. 2(b), each of the four DFB lasers in the array could be wavelength tuned by varying its operating current. The current tuning rate was around 0.016 nm/mA. The temperature tuning coefficient is about 0.1 nm/K (from −5 °C to 70 °C) when holding the current constant. Each laser had a tuning range of about 4 nm due to the current, and a maximum wavelength difference of 21.61 nm between DFB1 and DFB4 was achieved. No longitudinal mode hopping was observed during current tuning.

In operating the synthesiser system, THz electromagnetic waves would be created by mixing light from two of the four DFB lasers. Although the tuning ranges of the four DFB lasers are separated by several nanometres, DFG can be achieved continuously from 250 GHz to 2.7 THz, as shown in Fig. 3. The coloured regions denote all the possible frequencies bands that can be achieved by tuning the injection currents of the corresponding pairs of DFB lasers. From Fig. 3, the continuous THz tuning range could be separated into five channel regions (CRs), each with different redundancies as listed in [8]. A degree of redundancy makes the THz source suitable for applications where high reliability is mandatory, such as inter-satellite communications.

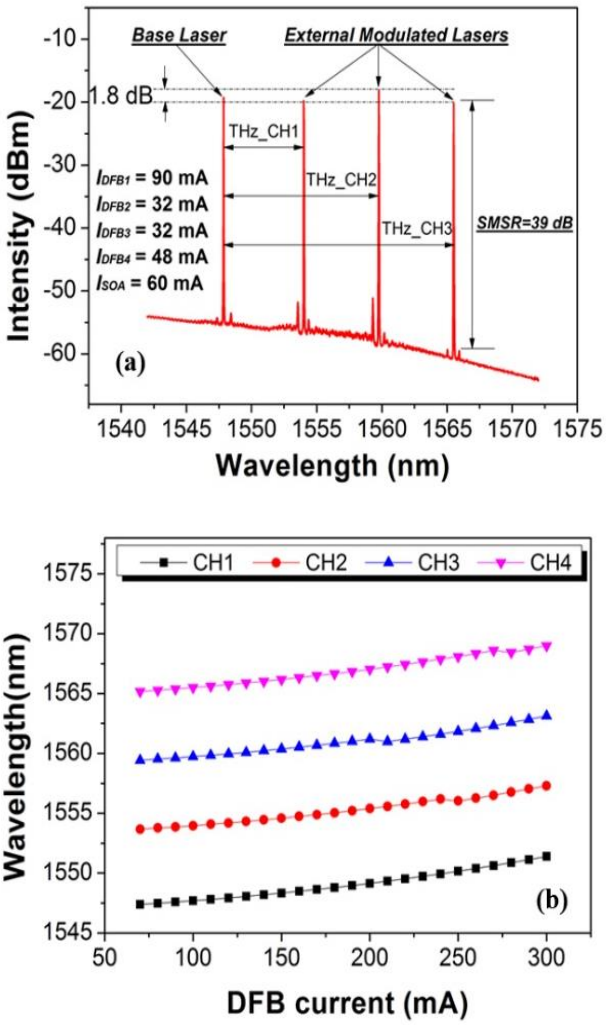

Fig. 2. THz channels established via laser array and individual DFB laser tunability at a temperature of 20 °C.

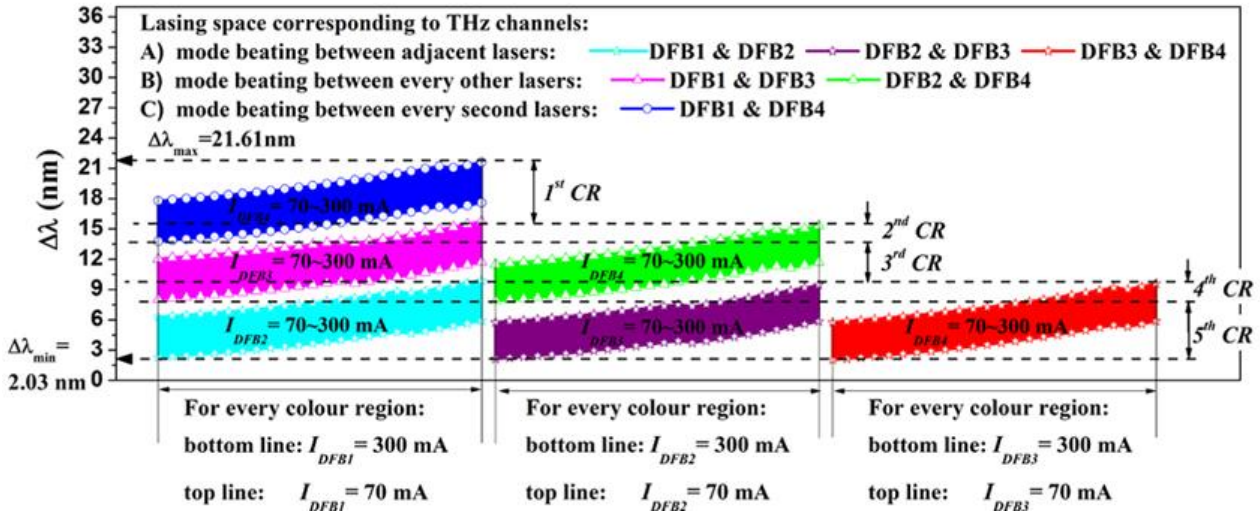

Fig.3 Continuous THz tuning using pairs of DFB lasers in the THz frequency synthesiser.

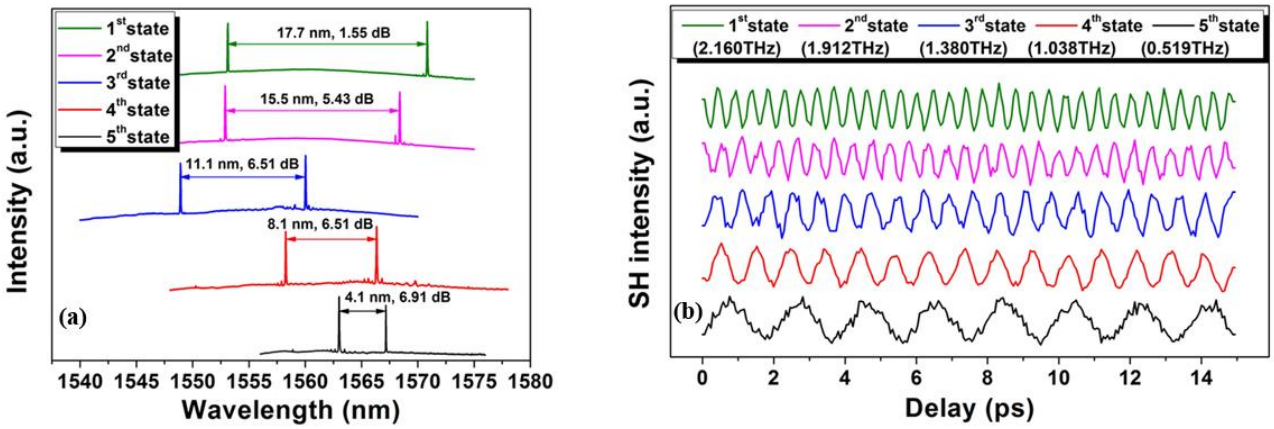

Fig. 4. Typical optical spectra and autocorrelation traces for the five CRs shown in Fig.3.

Figure 4 shows mode-beating optical spectra and the corresponding autocorrelation traces at five THz frequencies, one from each of the CRs shown in Fig. 3. Because of the narrow linewidth of the DFBs, the five second-harmonic generation (SHG) traces are essentially sinusoidal. The frequencies (0.519, 1.038, 1.380, 1.912, 2.160 THz) all lie within the ITU specified range for THz active services of 0.275 – 3.0 THz [15].

2.2. Dual-grating DFB integrated with EAM

A schematic of the laterally coupled dual-grating DFB laser integrated with an EAM, along with its dimensions and corresponding SEM images of the sidewall graing and cross-section of SEM, are shown in Fig. 5 [6, 9]. The mode beating frequency is determined principally by the laterally coupled grating periods on either side of the ridge waveguide and, critically, not by the ambient temperature or operation current. The EAM locks the phase of the two longitudinal modes through the four-wave mixing (FWM) effect.

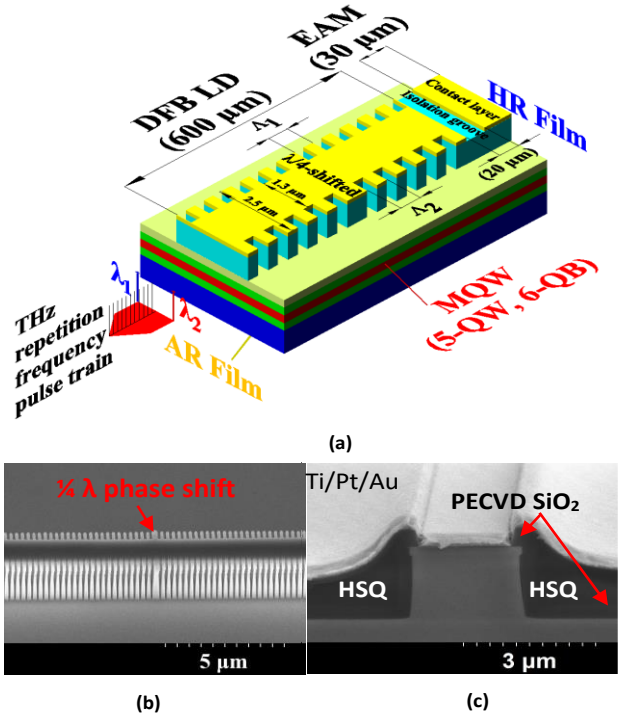

Fig.5. Schematic and SEM images of the dual-grating DFB laser/EAM device.

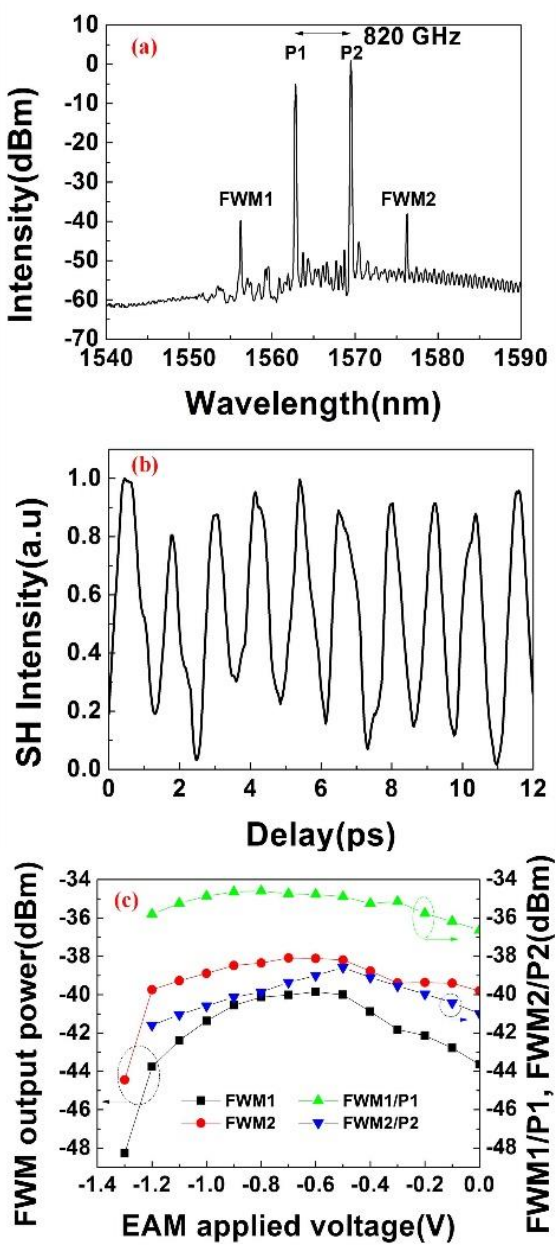

Fig. 6. Performance of the laterally-coupled dual-grating DFB device (a) optical spectrum, (b) autocorrelation trace, (c) dependence of the FWM output power on applied EAM voltage at I_{DFB} =100 mA and V_{EAM} = −0.6 V.

(a)

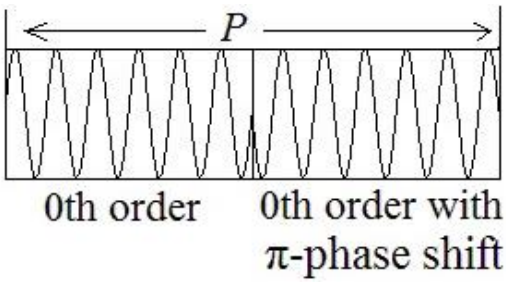

(b)

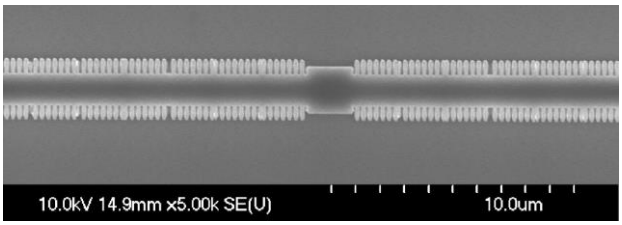

(c)

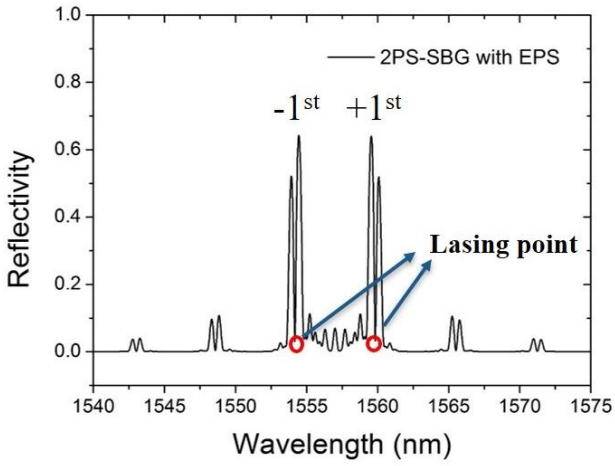

(d)

Fig.7. DFB diode laser based on π-phase-shifted sampled grating: (a) Micrograph of the fabricated device; (b) 2PS-SBG grating structure; (c) SEM image of the grating showing the EPS; (d) reflectivity spectrum of 2PS-SBG containing the EPS.

Figure 6 shows (a) the optical spectrum, (b) autocorrelation trace, and (c) the dependence of the FWM output power on the applied EAM voltage at a DFB injection current I_{DFB} =100 mA and EAM voltage V_{EAM} = −0.6 V. The two main longitudinal modes were at wavelengths of 1562.8 nm (P1) and 1569.5 nm (P2), corresponding to a frequency difference of 820 GHz, with a side mode suppression ratio (SMSR) >42 dB. The FWM sidebands at 1556.2 nm (FWM1) and 1576.3 nm (FWM2) are obvious with 15 dB power enhancements above the cavity modes, demonstrating good phase stability between the two main modes [16]. The autocorrelation trace is sinusoidal with an average period of 1.22 ps, which is exactly the reciprocal of the 820 GHz frequency difference. Figure 6(c) shows the dependence of the FWM output power on applied V_{EAM} [6] and demonstrates that the EAM plays a key role in terms of locking the phases of the two main longitudinal modes [17]. When the EAM voltage was tuned from 0 V to −1.3 V, the device operated in two stable longitudinal modes with prominent FWM peaks. This dual-grating DFB laser integrated with the nonlinear EAM could be used as a practical stable, compact solid-state laser source for generating THz radiation using a nonlinear optical crystal [18] or a photoconductive antenna (PCA) [4] as demonstrated in Section 2.3 below.

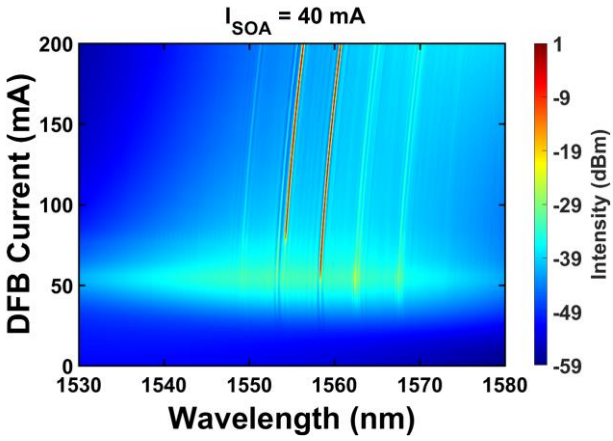

(a)

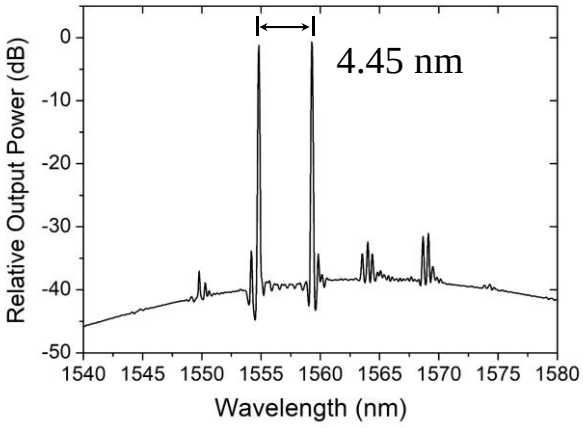

(b)

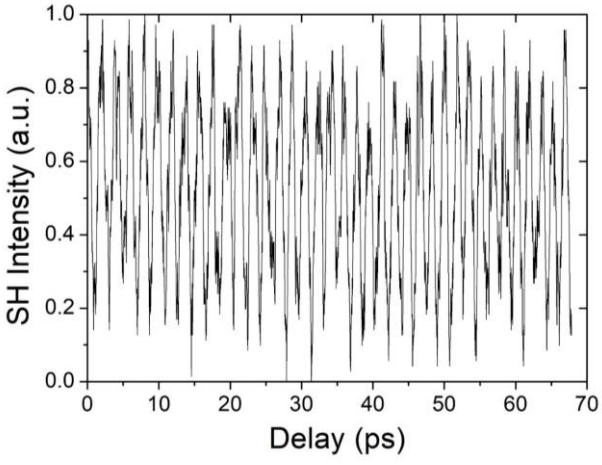

(c)

Fig. 8. The 2PS-SBG DWL performance.

2.3. *Dual-wavelength DFB diode laser based on π-phase-shifted sampled grating*

In contrast to Section 2.2 where a dual-period grating was used within the laser cavity, here a dual-wavelength DFB diode laser has been designed and fabricated based on a novel sampled Bragg grating (SBG). Both lasing wavelengths are generated simultaneously in the same DFB laser cavity and a 560 GHz beat signal is generated [10].

Figure 7(a) shows a micrograph of the fabricated device using shallow etched ridge waveguides and sidewall gratings [5, 8, 9]. The DFB section was 1200 μm long. In order to eliminate facet reflections, a 300 μm long curved SOA with an angle of 10° was introduced at the front output facet and a 125 μm long curved waveguide with an angle of 32° at the rear facet. The detailed structure is described in [10].

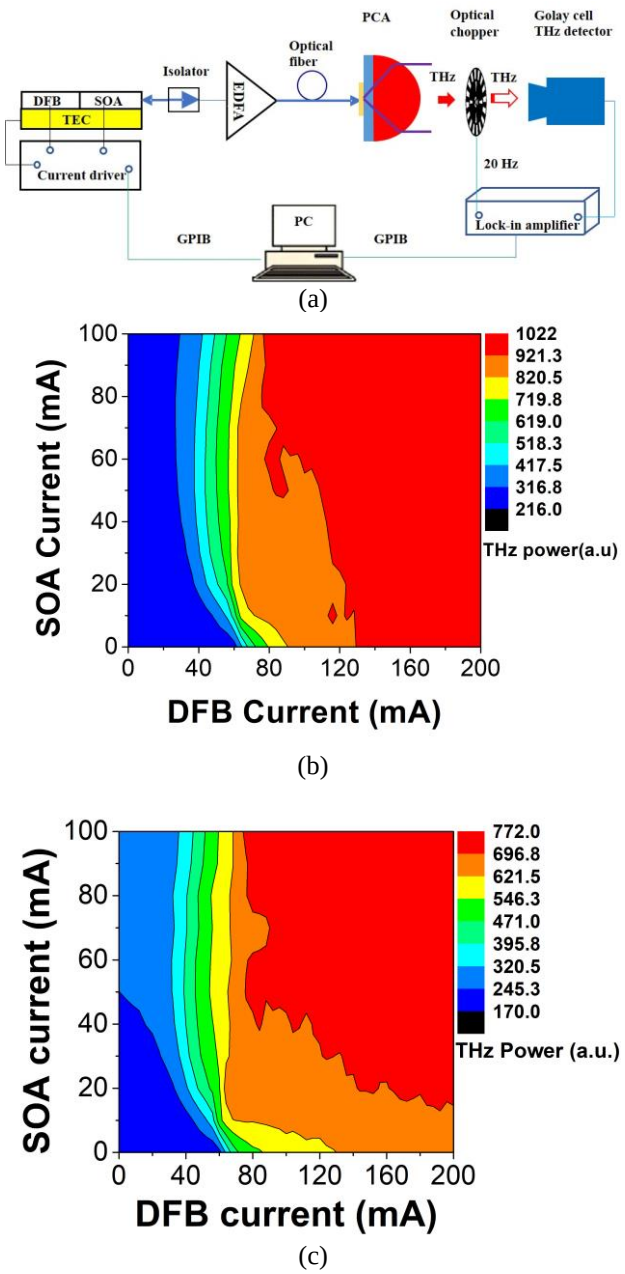

Fig. 9. The setup for THz signal measurement and measured results based on the 2PS-SBG DWL device. (a) Schematic of the THz generation and detection system; (b) detected THz signal with no white paper present in front of the THz detector; (c) detected THz signal with a white paper filter present in front of the THz detector.

The DWL here is based on a 2PS-SBG structure (Fig. 7(b)) [10]. For a conventional SBG with a 0.5 duty cycle, one half of every period has no grating. For the 2PS-SBG construction, the blank half period is filled with a π-phase-shifted grating; as a consequence, the ±1st-order reflections in the reflectivity spectrum are boosted and the 0th-order reflection disappears. By simply adjusting the sampling period, *P*, different wavelength spacings between the ±1st-order lasing modes can be achieved. When an equivalent π phase shift (EPS) [19] is introduced in the middle of the DFB laser cavity (Fig. 7(c)), single longitudinal mode lasing can be achieved simultaneously in each of the ±1st-order channels (Fig. 7(d)). A sampling period of 134.67 μm and seed grating period of 244 nm were used [10].

Figure 8(a) shows a 2D-wavelength map vs I_{DFB} with I_{SOA} = 40 mA. The threshold current is ~50 mA, and the ±1st-order peaks are stable over a large range of I_{DFB}. Fig. 8(b) shows the optical spectrum at I_{DFB} = 120 mA and I_{SOA} = 40 mA; the wavelength difference between the ±1st-order lasing modes is 4.45 nm with a power difference less than 0.5 dB and SMSR more than 30 dB [10]. Fig. 8(c) shows the corresponding autocorrelation trace which has a 1.8 ps average emitted pulse period, exactly the reciprocal of the beat frequency of 560 GHz.

Figure 9(a) shows a schematic of the setup used to generate and detect the THz signal based on the 2PS-SBG DWL. The output light from the DWL was coupled into a lensed fibre, passed through an isolator, then amplified by an erbium-doped fibre amplifier (EDFA) to pump a PCA and so generate THz signals using the photomixing effect. The output light from the DWL was amplified to an average power of 24 mW by the EDFA, just below the maximum power specified for the PCA. The PCA was operated with a bias voltage of 10 V. The THz waves were then incident on a Golay cell. A lock-in amplifier (LIA) combined with an optical chopper was used to extract the small THz signal from the noisy measurement environment. The optical chopper, driven at a 20 Hz modulation frequency, was placed after the PCA emitter. The current drivers on the DFB and SOA sections, and the signal extraction from the LIA were automated, being controlled by a personal computer (PC) MATLAB program using the general purpose interface bus (GPIB) interface [10].

Figure 9(b) shows a 2D-power map of the THz signal vs I_{DFB} and I_{SOA}. I_{DFB} and I_{SOA} were scanned from 0 mA to 200 mA and from 0 mA to 100 mA respectively. Stable THz signals were detected over a wide range of I_{DFB} and I_{SOA} which confirms the simultaneous stable lasing at two wavelengths shown in Fig. 8(a).

The highest detected THz power was about 30 nW. There are two reasons which lead to the relatively low THz power. One is the low optical-to-THz conversion efficiency at room temperature of the PCA, which is around 10^{-5} [18]. The second reason is that only about 10% of the THz signal was collected by the Golay cell due to the following: the 30° divergence angle of radiation from the PCA; the distance (140 mm) between the PCA and the entrance of the Golay cell detector; and the 11 mm diameter of the entrance cone of the detector. Taking these factors into consideration, the total THz output power is estimated to be around 1.4 μW [20].

The Golay cell is sensitive to an exceptionally wide range of wavelengths, from at least 1 μm to 8 mm. To confirm that the detected signal was mainly due to THz radiation and not, for example, leakage of 1.5 μm radiation from the diode laser, a sheet of white paper with a density of 80 g/m^2 was positioned between the optical chopper and the Golay cell. The measured 2D-power map of the THz signal is shown in Fig. 9(c), with I_{DFB} and I_{SOA} scanned from 0 mA to 200 mA and from 0 mA to 100 mA respectively. Compared to Fig. 9(b) without the paper, the detected power with the paper was reduced by about 24.5% at the highest power points, which is probably caused by scattering from the surface of the paper [21]. Most of the THz power was transmitted through the paper, which is consistent with the transmission property of THz waves. Separate measurements showed that the transmission of 1.5 μm radiation through the paper is <10%, confirming that leakage of 1.55 μm laser radiation could not be responsible for more than a small fraction of the signal detected by the Golay cell.

2.4. SGDBR SMLLD

In contrast to the PIC devices reported in Section 2.1-2.3, here we introduce a 1.55 μm SMLLD operating in the THz band, in this case at 640 GHz. This device uses a conventional SGDBR structure, and the SMLLD exhibits highly controllable and robust mode-locked operation, with stable mode locking observed over a wide range of bias parameters. The SGDBR structure provides strong selectivity of optical modes separated by the desired mode locking frequency, while the distributed reflectors relax fabrication tolerances enabling the cavity to self-adjust to support an integral number of mode locked pulses. In contrast, in conventional colliding pulse mode locked (CPM) [22] and compound cavity mode locked (CCM) THz LDs [23, 24], the cavity cleaving accuracy is critical in enabling high-quality harmonic mode-locking (HML). For example, 1.5 THz mode locking has been reported using the CCM method in DBR lasers [23]. Unfortunately, the operation range in terms of parameters such as gain current and saturable absorber (SA) voltage is very narrow. Furthermore, these CCM THz LDs have limited reproducibility. CCM Fabry-Perot (FP) LDs incorporating an intra-cavity reflector (ICR) demonstrated mode locking at 2.1 THz in the 850 nm wavelength range [24]. However, the mode locked frequency of this device depends critically on the accuracy of the positioning of the ICR within the cavity, because the length of the long cavity must be an exact integer multiple, within a very tight tolerance, of that of the short cavity.

The 640 GHz SGDBR SMLLD device structure and dimensions are the same as reported in [11] and are shown in Fig. 10(a). The SMLLD has three functional sections: the saturable absorber (SA) phase locking section (30 μm), the gain section (960 μm), the SGDBR section (675 μm with ten sampled grating periods). The round trip time of the 67.5 μm sampled grating period corresponds to the mode locking frequency of 640 GHz. The system used to generate and detect THz radiation was similar to that shown in Fig. 9(a) with the SA side facing the isolator. Compared to the DWL measurement, an additional probe was required to characterise the SMLLD. The three probes were used to apply currents to the gain section (I_{Gain}) and the SGDBR section (I_{SGDBR}), and a reverse bias voltage to the SA section (V_{SA}).

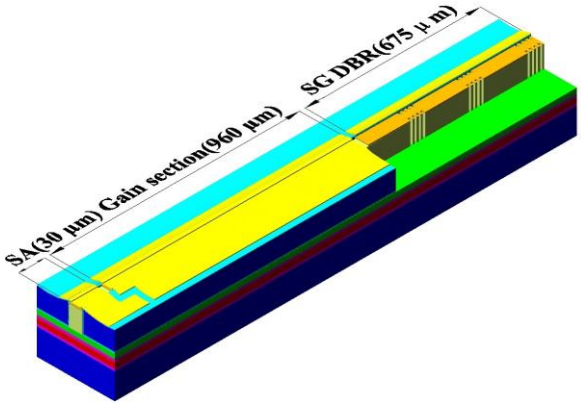

(a)

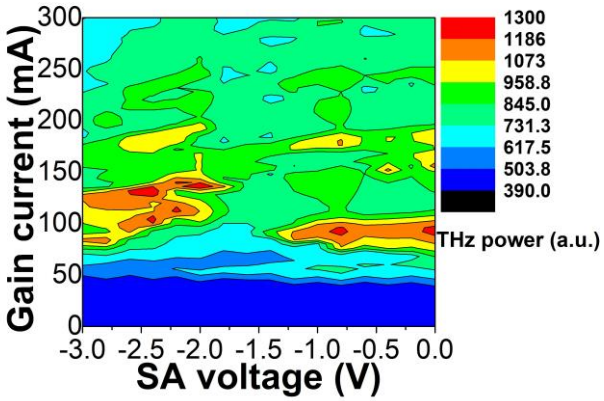

(b)

Fig. 10. SGDBR SMLLD device structure and THz signal measured results based on the SGDBR SMLLD device. (a) Schematic diagram of the 1.55 μm SGDBR SMLLD; (b) 2-dimensional plots of the THz power vs I_{Gain} and V_{SA} at I_{SGDBR} = 0 mA, with no white paper present in front of the 640 GHz band pass filter.

Another difference in the setup was that a 640 GHz band pass filter was placed between the chopper and the Golay cell to prevent unwanted radiation, including 1.55 μm light from the laser, entering the THz detector [12].

Figure 10(b) shows a 2-dimensional map of the measured THz power vs I_{Gain} and V_{SA} in the case of I_{SGDBR} = 0 mA. The platform seen in the THz power, with a value of about 390 arbitrary units, stems from amplified spontaneous emission noise from the EDFA itself. With the laser biased under mode locking conditions, significant THz powers above the noise floor were detected across a wide operating range, i.e., 50 mA $\leqslant I_{Gain} \leqslant$ 300 mA and −3 V $\leqslant V_{SA} \leqslant$ 0 V. There are two regions which have the highest THz signal intensity. The first lies in the region defined by −3 V $\leqslant V_{SA} \leqslant$ −1.8 V and 80 mA $\leqslant I_{Gain} \leqslant$ 144 mA, and the other where −1.2V $\leqslant V_{SA} \leqslant$ 0 V and 80 mA $\leqslant I_{Gain} \leqslant$ 100 mA [9]. The highest detected THz power is about 20 nW according to our absolute power calibration. The factors leading to the relatively low detected THz power have already been discussed in Section 2.3. Taking account of the divergence angle of THz beam and collection angle of the detector, the true THz output power is estimated to be around 0.2 μW.

To increase the THz power in future, we plan to use uni-travelling-carrier photodiodes (UTC-PDs), which operate

with better efficiency at high frequencies than other photomixers [25]. We also note that a semiconductor optical amplifier can readily reach the saturation powers of photodiode and PCA detectors, eliminating the need for the EDFA used in the present measurements.

3. Conclusion

In this paper four kinds of PIC used to produce THz signals have been reported. A PIC-based optoelectronic frequency synthesiser for THz communications, integrating 4 DFB lasers, could be tuned continuously from 0.254 to 2.723 THz. A 1.55 μm dual-grating DFB laser integrated with a nonlinear EAM device generated a beat signal at 820 GHz, with FWM in the EAM stabilising the operation of the device. A dual-wavelength DFB diode laser, incorporating a novel 2 section phase shift sampled grating, was used along with a PCA to generate a THz electromagnetic wave at 560 GHz. This device exhibited stable DWL performance over a wide range of drive current. Finally, stable mode locking at THz repetition frequencies, again over a wide range of bias parameters, was demonstrated using a DBR laser with conventional sampled gratings. A THz electromagnetic wave at 640 GHz was generated based on this laser and PCA system.

4. Acknowledgements

This work was supported in part by the U.K. Engineering and Physical Sciences Research Council under Grant EP/R042578/1 and by the National Science Foundation of China under Grant 61320106013.

5. References

[1] Zhang, X., 'Terahertz wave imaging: horizons and hurdles', Physics in Medicine and Biology, 2002, **47**, (21), p. 3667

[2] Hangyo, M., Nagashima, T., and Nashima, S., 'Spectroscopy by pulsed terahertz radiation', Measurement Science and Technology, 2002, **13**, (11), p. 1727

[3] Hu, B. and Nuss, M., 'Imaging with terahertz waves', Optics Letters, 1995, **20**, (16), pp. 1716-1718

[4] Tani, M., Gu, P., Hyodo, M., Sakai, K., and Hidaka, T., 'Generation of coherent terahertz radiation by photomixing of dual-mode lasers', Optical and Quantum Electronics, 2000, **32**, (4), pp. 503-520

[5] Yang, S.-H., Watts, R., Li, X., Wang, N., Cojocaru, V., O'Gorman, J., Barry, L., and Jarrahi, M., 'Tunable terahertz wave generation through a bimodal laser diode and plasmonic photomixer', Optics Express, 2015, **23**, (24), pp. 31206-31215

[6] Hou, L., Haji, M., Eddie, I., Zhu, H., and Marsh, J.H., 'Laterally coupled dual-grating distributed feedback lasers for generating mode-beat terahertz signals', Optics Letters, 2015, **40**, (2), pp. 182-185

[7] Osborne, S., O'Brien, S., Buckley, K., Fehse, R., Patchell, J., Kelly, B., O'Gorman, J., and O'Reilly, E., 'Two-colour Fabry-Perot laser with terahertz primary mode spacing', Electronics Letters, 2007, **43**, (4), pp. 224-225

[8] Xu, J., Hou, L., Deng, Q., Han, L., Liang, S., Marsh, J.H., and Zhu, H., 'Fully integrated multi-optoelectronic synthesizer for THz pumping source in wireless communications with rich backup redundancy and wide tuning range', Scientific Reports, 2016, **6**, 29084

[9] Hou, L., Haji, M., Eddie, I., Zhu, H., and Marsh, J.H., 'Laterally-coupled dual-grating distributed feedback lasers for generating mode-beat terahertz signals', in, Conference on Lasers and Electro-Optics: 2015, (Optical Society of America, 2015)

[10] Tang, S., Hou, B., Liang, S., Chen, D., Hou, L., and Marsh, J.H., 'Terahertz signal generation based on a dual-mode 1.5 μm DFB semiconductor laser', in, Conference on Lasers and Electro-Optics/Pacific Rim, (Optical Society of America, 2018)

[11] Hou, L., Haji, M., and Marsh, J.H., 'Mode locking at terahertz frequencies using a distributed Bragg reflector laser with a sampled grating', Optics Letters, 2013, **38**, (7), pp. 1113-1115

[12] Hou, L., Hou, B., Liang, S., Chen, D., and Marsh, J.H., 'Generation of THz radiation by sampled grating DFB mode locked laser diodes', in Conference on Lasers and Electro-Optics/Pacific Rim, (Optical Society of America, 2018)

[13] Hou, L., Haji, M., Qiu, B., and Bryce, A.C., 'Mode-locked laser array monolithically integrated with MMI combiner, SOA, and EA modulator', IEEE Photonics Technology Letters, 2011, **23**, (15), pp. 1064-1066

[14] Hou, L., Stolarz, P., Javaloyes, J., Green, R.P., Ironside, C.N., Sorel, M., and Bryce, A.C., 'Subpicosecond pulse generation at quasi-40-GHz using a passively mode-locked AlGaInAs–InP 1.55 μm strained quantum-well laser', IEEE Photonics Technology Letters, 2009, **21**, (23), pp. 1731-1733

[15] Report ITU-R SM.2352-0, 'Technology trends of active services in the frequency range 275-3 000 GHz' (International Telecommunication Union, Geneva, 2015)

[16] Klehr, A., Fricke, J., Knauer, A., Erbert, G., Walther, M., Wilk, R., Mikulics, M., and Koch, M., 'High-power monolithic two-mode DFB laser diodes for the generation of THz radiation', IEEE Journal of Selected Topics in Quantum Electronics, 2008, **14**, (2), pp. 289-294

[17] Mori, T. and Kawaguchi, H., 'Characteristics of nondegenerate four-wave mixing in electroabsorption modulator', Applied Physics Letters, 2004, **85**, (6), pp. 869-871

[18] Yang, Z., Mutter, L., Stillhart, M., Ruiz, B., Aravazhi, S., Jazbinsek, M., Schneider, A., Gramlich, V., and Günter, P., 'Large-size bulk and thin-film stilbazolium-salt single crystals for nonlinear optics and THz generation', Advanced Functional Materials, 2007, **17**, (13), pp. 2018-2023

[19] Shi, Y., Li, S., Chen, X., Li, L., Li, J., Zhang, T., Zheng, J., Zhang, Y., Tang, S., Hou, L., Marsh, J.H., and Qiu, B, 'High channel count and high precision channel spacing multi-wavelength laser array for future PICs', Scientific Reports, 2014, **4**, 7377

[20] Gupta, A., Rana, G., Bhattacharya, A., Singh, A., Jain, R., Bapat, R.D., Duttagupta, S., and Prabhu, S., 'Enhanced optical-to-THz conversion efficiency of photoconductive antenna using dielectric nano-layer encapsulation', APL Photonics, 2018, **3**, (5), pp. 051706

[21] Tang, S.: 'InP-based semiconductor lasers with novel sampled Bragg gratings and applications', PhD thesis University of Glasgow, 2019
[22] Shimizu, T., Ogura, I., and Yokoyama, H., '860 GHz rate asymmetric colliding pulse modelocked diode lasers', Electronics Letters, 1997, **33**, (22), pp. 1868-1869
[23] Arahira, S., Matsui, Y., and Ogawa, Y., 'Mode-locking at very high repetition rates more than terahertz in passively mode-locked distributed-Bragg-reflector laser diodes', IEEE Journal of Quantum Electronics, 1996, **32**, (7), pp. 1211-1224
[24] Yanson, D.A., Street, M.W., McDougall, S.D., Thayne, L., Marsh, J.H., and Avrutin, E.A., 'Ultrafast harmonic mode-locking of monolithic compound-cavity laser diodes incorporating photonic-bandgap reflectors', IEEE Journal of Quantum Electronics, 2002, **38**, (1), pp. 1-11
[25] Song, H.-J., Ajito, K., Muramoto, Y., Wakatsuki, A., Nagatsuma, T., and Kukutsu, N., 'Uni-travelling-carrier photodiode module generating 300 GHz power greater than 1 mW', IEEE Microwave and Wireless Components Letters, 2012, **22**, (7), pp. 363-365